


Spectral solar irradiance on inclined surfaces: A fast Monte Carlo approach

Cite as: J. Renewable Sustainable Energy **12**, 053705 (2020); <https://doi.org/10.1063/5.0011635>
Submitted: 22 April 2020 . Accepted: 16 September 2020 . Published Online: 14 October 2020

Mengying Li , Zhouyi Liao , and Carlos F. M. Coimbra 

COLLECTIONS

 This paper was selected as Featured



View Online



Export Citation



CrossMark

ARTICLES YOU MAY BE INTERESTED IN

[Clear-sky index space-time trajectories from probabilistic solar forecasts: Comparing promising copulas](#)

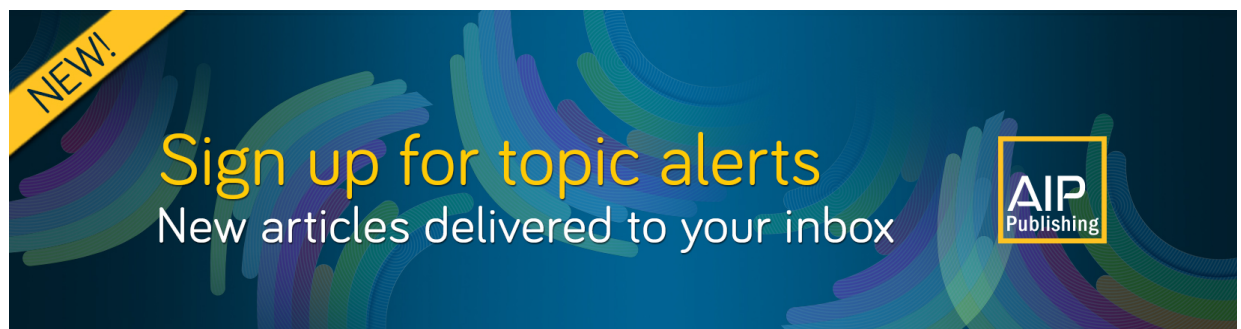
Journal of Renewable and Sustainable Energy **12**, 026102 (2020); <https://doi.org/10.1063/1.5140604>

[Satellite-augmented diffuse solar radiation separation models](#)

Journal of Renewable and Sustainable Energy **11**, 023705 (2019); <https://doi.org/10.1063/1.5087463>


[Standard of reference in operational day-ahead deterministic solar forecasting](#)

Journal of Renewable and Sustainable Energy **11**, 053702 (2019); <https://doi.org/10.1063/1.5114985>



NEW!

Sign up for topic alerts
New articles delivered to your inbox



Spectral solar irradiance on inclined surfaces: A fast Monte Carlo approach

Cite as: J. Renewable Sustainable Energy **12**, 053705 (2020); doi: [10.1063/5.0011635](https://doi.org/10.1063/5.0011635)

Submitted: 22 April 2020 · Accepted: 16 September 2020 ·

Published Online: 14 October 2020



View Online



Export Citation



CrossMark

Mengying Li,  Zhouyi Liao,  and Carlos F. M. Coimbra^{a)} 

AFFILIATIONS

Department of Mechanical and Aerospace Engineering, Jacobs School of Engineering, Center of Excellence in Renewable Resource Integration and Center for Energy Research, University of California San Diego, 9500 Gilman Drive, La Jolla, California 92093, USA

^{a)} Author to whom correspondence should be addressed: ccoimbra@ucsd.edu

ABSTRACT

Estimating spectral plane-of-array (POA) solar irradiance on inclined surfaces is an important step in the design and performance evaluation of both photovoltaic and concentrated solar plants. This work introduces a fast, line-by-line spectral, Monte Carlo (MC) radiative transfer model approach to simulate anisotropic distributions of shortwave radiation through the atmosphere as photon bundles impinge on inclined surfaces. This fast Monte Carlo approach reproduces the angular distribution of solar irradiance without the undesirable effects of spatial discretization and thus computes detailed POA irradiance values on surfaces at any orientation and also when surfaces are subjected to the anisotropic ground and atmospheric scattering. Polarization effects are also easily incorporated into this approach that can be considered as direct numerical simulation of the physics involved. Here, we compare our Monte Carlo radiative transfer model with the most widely used empirical transposition model, Perez4, under various conditions. The results show that the Perez4 model reproduces the more detailed Monte Carlo simulations with less than 10% deviation under clear skies for all relevant surface tilt and azimuth angles. When optically thin clouds are present, observed deviations are larger, especially when the receiving surface is strongly tilted. Deviations are also observed for large azimuth angle differences between the receiving surface and the solar position. When optically thick clouds are present, the two models agree within 15% deviation for nearly all surface orientation and tilt angles. The overall deviations are smaller when compared with cases for optically thin clouds. The Perez4 model performs very well (~6.0% deviation) in comparison with the detailed MC simulations for all cases, thus validating its widespread use for practical solar applications. When detailed atmospheric profiles and cloud optical properties are available, the proposed fast Monte Carlo radiative model reproduces accurate spectral and angular POA irradiance levels for various atmospheric and cloud cover conditions, surface orientations, and different surface and ground properties.

Published under license by AIP Publishing. <https://doi.org/10.1063/5.0011635>

I. INTRODUCTION

The design and performance evaluation of photovoltaic (PV) and concentrated solar power systems requires the determination of plane of array (POA) solar irradiation on inclined surfaces.¹ For example, to maximize the power output of fixed tilt photovoltaic arrays, year-around POA irradiance values on surfaces with different orientations are used to find the optimal tilt and azimuth angles for photovoltaic (PV) panels.² Those calculations typically require cloud cover estimates and can be made quite accurately if the optical properties of the local atmosphere and of the surrounding ground are well characterized. PV panels, and to a much lesser extent, reflective mirrors, respond only to certain wavelengths in the solar spectrum,³ so the characterization of spectral POA irradiance is also of practical and economic interest for the operation of solar farms.

Various transposition models^{4–8} have been proposed in the literature to derive POA irradiance from global horizontal irradiance (GHI), diffuse horizontal irradiance, direct normal irradiance (DNI), and foreground albedo values. The earliest transposition models assume sky diffuse irradiance to be isotropic,⁴ but in reality, the scattering by gas molecules, aerosols, and clouds is mostly anisotropic.⁹ Subsequently, more sophisticated empirical models were proposed to treat the effects of anisotropy in sky diffuse irradiance.^{5–8} The coefficients in most of the transposition models are regressed from local measurements, so the accuracy of these models may vary with local meteorological conditions, such as vertical profiles of atmospheric gases, aerosol types and loading, cloud types and optical properties, and relative angles between the solar beam and the surface.^{1,10–12} In general, transposition models are also less accurate for larger surface tilting angles (i.e., approaching 90° with the horizontal plane).¹

To obtain accurate POA irradiance values, detailed atmospheric radiative transfer models are typically needed.^{13–16} For longwave radiative transfer in the atmosphere ($\lambda > 4 \mu\text{m}$), a two-flux spectral multilayer model has been previously developed by the authors¹⁷ to calculate the downwelling and upwelling flux densities in the atmosphere at a spectral resolution of 0.01 cm^{-1} . The two-flux model is sufficiently accurate for longwave radiative transfer because the emission from the atmosphere and ground is mostly diffuse and nearly isotropic. However, for solar shortwave radiative transfer ($\lambda < 4 \mu\text{m}$), the radiation source is strongly directional, and most approaches rely on discrete-ordinate models with multiple streams (e.g., eight-streams or 16-streams) to model the angular-dependent solar intensity.¹⁵ Discrete-ordinate models (DOMs) solve the integrodifferential radiative transfer equation (RTE) using a discrete hemispheric sum and then employ linear algebra methods to solve the discretized equations numerically.¹⁸ The fidelity of DOMs increases with the number of streams, but the complexity of the numerical code and the computational cost involved increase as well. For plane-parallel models of the atmosphere, DOMs such as the popular DISORT (Discrete Ordinates Radiative Transfer Program for a Multi-Layered Plane-Parallel Medium)^{18,19} are known to be computationally efficient and have been widely used in the atmospheric physics literature.^{16,20}

The problem at hand is not new. Approximations for shortwave irradiance on inclined surfaces typically rely on parametric models that account for clear skies only [e.g., the Simple Model of the Atmospheric Radiative Transfer of Sunshine (SMARTS)^{21,22} approach] or on radiative transfer models that allow for the approximation of diffuse and direct radiative fluxes under cloudy conditions [e.g., the Fast All-Sky Radiation Model for Solar applications with Narrowband Irradiances on Tilted surfaces (FARMS-NIT) approach²³]. In general, parametric models use the different horizontal (global and diffuse) or direct normal components of the solar irradiance as inputs to more detailed narrowband calculations. Fast radiative models use clear sky estimates for those shortwave components to simulate the effects of clouds on spectral fluxes. Such approaches provide fast and reliable results that are often within the range of tolerances needed for the design and evaluation of solar power plants.²²

Another approach to model accurately the shortwave radiative transfer through the atmosphere and onto inclined surfaces is to employ physically based Monte Carlo (MC) methods. MC methods employ statistical sampling to simulate the actual transport of representative photons through the medium instead of solving RTEs based on beam discretization. The ultimate goal of the line of research introduced in the present work is the development of carefully validated MC radiative models that are able to tackle complex three-dimensional cloud and surface geometries.

The MC method is substantially simpler to code and implement and reproduces high levels of physical realism (including complex geometrical paths and the effects of polarization, anisotropy, and multiple scattering²⁴). Until recently, MC methods were not extensively used for practical applications only because of their poor scalability with respect to resolution (number of photon bundles needed). However, given the recent advances in Graphics Processing Unit (GPU) acceleration and parallel computational power, there are substantial advantages in using MC simulations due to coding simplicity and the ability to produce high-fidelity (direct numerical simulation) results for both two- and three-dimensional geometries.

In this work, we develop a two-dimensional MC radiative model to compute spectral solar irradiance on an inclined surface. We compare and validate the accuracy of current parametric transposition models after detailed validation of the MC code itself. Section II presents the radiative model in detail. Section III includes a short description of the validation of the MC radiative model. The results and discussion of spectral solar irradiance on inclined surfaces and a performance comparison of selected empirical transposition model are presented in Sec. IV. Conclusions follow in Sec. V.

II. THE RADIATIVE MODEL

We consider a solar spectral range from 2500 cm^{-1} to 35000 cm^{-1} ($0.286 \mu\text{m}$ to $4 \mu\text{m}$). The atmosphere is modeled as a number of plane-parallel layers extending from the ground to the top-of-atmosphere (TOA, 120 km above the ground). The different layers are divided using pressure coordinates.¹⁷ The temperature and atmospheric gas profiles are assumed to follow Air Force Geophysics Lab (AFGL) midlatitude summer profiles,²⁵ with gas profiles corrected for current surface concentrations.¹⁷ The ozone concentration on the surface is corrected to 50 ppb.^{26,27} The spectral absorption coefficients of gas molecules are retrieved from the HITRAN database,²⁸ and the continuum absorption coefficients of water vapor, carbon dioxide, ozone, and oxygen are calculated using the MT_CKD continuum model.²⁹ Ozone and oxygen continuum absorption are added in the shortwave model because their effect is more significant in the shortwave than in the longwave spectrum. The absorption, scattering coefficients, and asymmetry parameters of aerosols and water clouds are calculated via approximations based on Mie theory taking into consideration proper size distributions.^{17,30} Ice clouds are not considered in the current model. The scattering of gas molecules is neglected in the longwave spectrum but is modeled as Rayleigh scattering in the shortwave spectrum.⁹

A. Monochromatic extinction coefficients

The Rayleigh scattering coefficient is calculated as³¹

$$\kappa_{s,\text{gas}} = \frac{24\nu^4 N \pi^3 (n_s^2 - 1)^2 F_k}{N_s^2 (n_s^2 + 2)^2}, \quad (1)$$

where ν (cm^{-1}) is the wavenumber; N (cm^{-3}) and N_s ($2.54743 \times 10^{19} \text{ cm}^{-3}$) are the molecular number densities of current and standard air, respectively; n_s is the refractive index for standard air at wavenumber ν ; and F_k is the King corrector factor defined as $(6 + 3\rho_n)/(6 - 7\rho_n)$, where ρ_n is the depolarization factor at the wavenumber ν that accounts for the anisotropy of the air molecules.³¹

The wavenumber-dependent refractive index of standard air in the shortwave spectrum is approximated as³²

$$(n_s - 1) \times 10^8 = \frac{5791817}{238.0185 - (\nu/10^4)^2} + \frac{167909}{57.362 - (\nu/10^4)^2}. \quad (2)$$

The molecular number density of the atmospheric layer under consideration is calculated from the ideal gas law using layer averaged temperatures and pressures.

Figure 1 shows the absorption (solid) and scattering (dashed) coefficients of atmospheric gases, aerosols, and clouds in the lowest atmospheric layer used in the model. For the standard cases, the optical depth of aerosols [aerosol optical depth (AOD)] and clouds [cloud

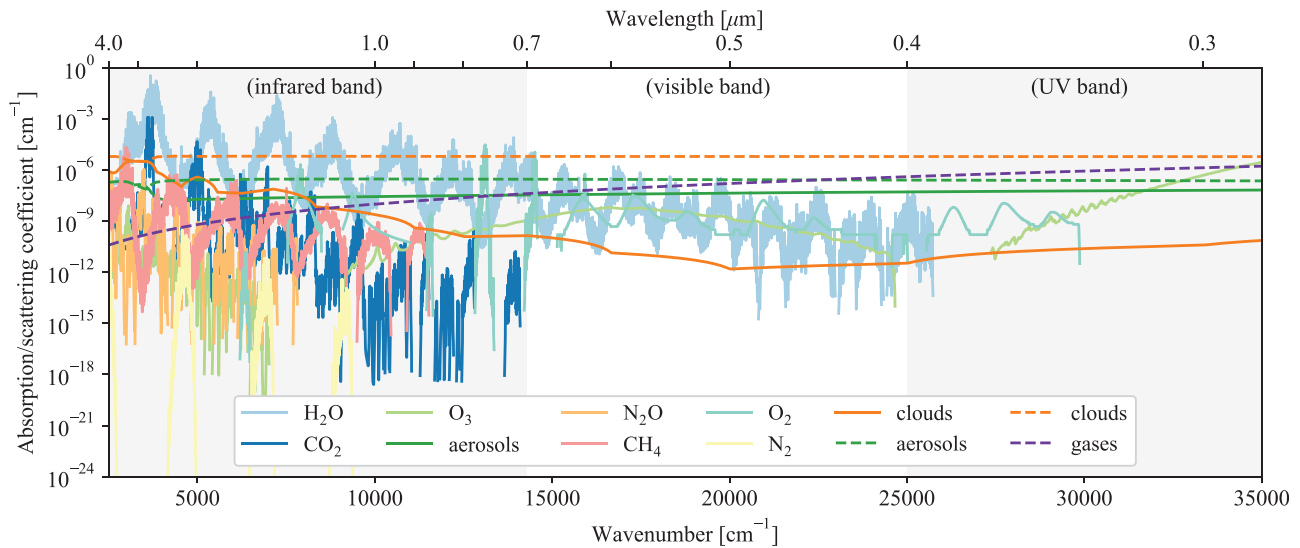


FIG. 1. Spectral absorption (solid lines) and scattering (dashed lines) coefficients for main atmospheric constituents at the lowest layer of the troposphere. AODs and CODs at 497.5 nm with a scale height of 1575 m (Ref. 17) are set to be 0.05 and 1.0, respectively.

optical depth (COD)] at 497.5 nm are set to be 0.05 and 1.0, respectively. Ozone absorption dominates the UV spectrum, while water vapor absorption dominates the near infrared spectrum. In the visible range of the spectrum, scattering by gas molecules and absorption/scattering of aerosols and clouds dominate the radiative process.

B. Zenith angle correction

When the solar zenith angle is greater than 70°, refraction in the atmosphere and the Earth’s curvature effects are considered. The air mass for different solar zenith angles is given by^{33,34}

$$\begin{aligned} \theta_z < 70^\circ: \text{AM} &= \frac{1}{\cos\theta_z}, \\ \theta_z > 70^\circ: \text{AM} &= \frac{\exp(-0.001184z_0)}{\cos\theta_z + 0.5057(96.080 - \theta_z)^{-1.634}}, \end{aligned} \quad (3)$$

where θ_z (°) is the solar zenith angle and z_0 (m) is the altitude of local stations. To account for air mass effects, the solar zenith angle is corrected as an input to the MC model,

$$\theta_z^* = \cos^{-1}(1/\text{AM}). \quad (4)$$

Note that the corrected solar zenith angle θ_z^* is smaller than the real θ_z when $\theta_z > 70^\circ$.

C. A fast Monte Carlo method

In what follows, a Monte Carlo method to simulate the transport of photons in the earth-atmosphere domain²⁴ is described in detail. For each wavenumber bandwidth, the monochromatic upwelling and downwelling flux densities are calculated by tracing the paths of a large number of photons. The energy carried by each photon is given by

$$e_\nu = \frac{G_{0,\nu} \cos\theta_z}{N_b}, \quad (5)$$

where $G_{0,\nu}$ is the monochromatic extraterrestrial solar flux density at the central wavenumber ν , θ_z is the solar zenith angle, and N_b is the number of photons used for each wavenumber bandwidth. The extraterrestrial solar flux density is retrieved from the 2000 ASTM Standard Extraterrestrial Spectrum.³⁵

Figure 2 shows a code flow chart for the fast MC radiative transfer model, where processes in the rectangles with thick lines make use random number generators. Photons enter the earth-atmosphere system from the top-of-atmosphere (TOA) in the direction of (r_x, r_y, r_z) determined by the solar zenith θ_z and azimuth angles γ_{az}

$$r_x = \sin\theta_z \cos\gamma_{az}, \quad r_y = \sin\theta_z \sin\gamma_{az}, \quad r_z = \cos\theta_z. \quad (6)$$

When traveling through the atmosphere, photons may collide with atmospheric particles (molecules, aerosols, and cloud droplets) and then be either absorbed or scattered. A new photon bundle enters the system after the life of the previous photon bundle ends. The total number of photons is predefined to reach an optimal balance between accuracy and computational cost (see Sec. III A for details).

1. Photon transport

The probability that a photon travels through an optical depth τ without collision is

$$p(\tau)d\tau = e^{-\tau}d\tau. \quad (7)$$

Then, the optical depth a photon travels before the next collision τ_0 is sampled by inverting the cumulative probability function,

$$\begin{aligned} \xi_{\tau_0} &= \int_0^{\tau_0} e^{-\tau}d\tau = 1 - e^{-\tau_0}, \\ \tau_0 &= -\ln(1 - \xi_{\tau_0}) = -\ln\xi_{\tau_0}, \end{aligned} \quad (8)$$

where ξ_{τ_0} is a random number uniformly sampled from 0 to 1 (all ξ values in this work are uniformly sampled random real numbers from

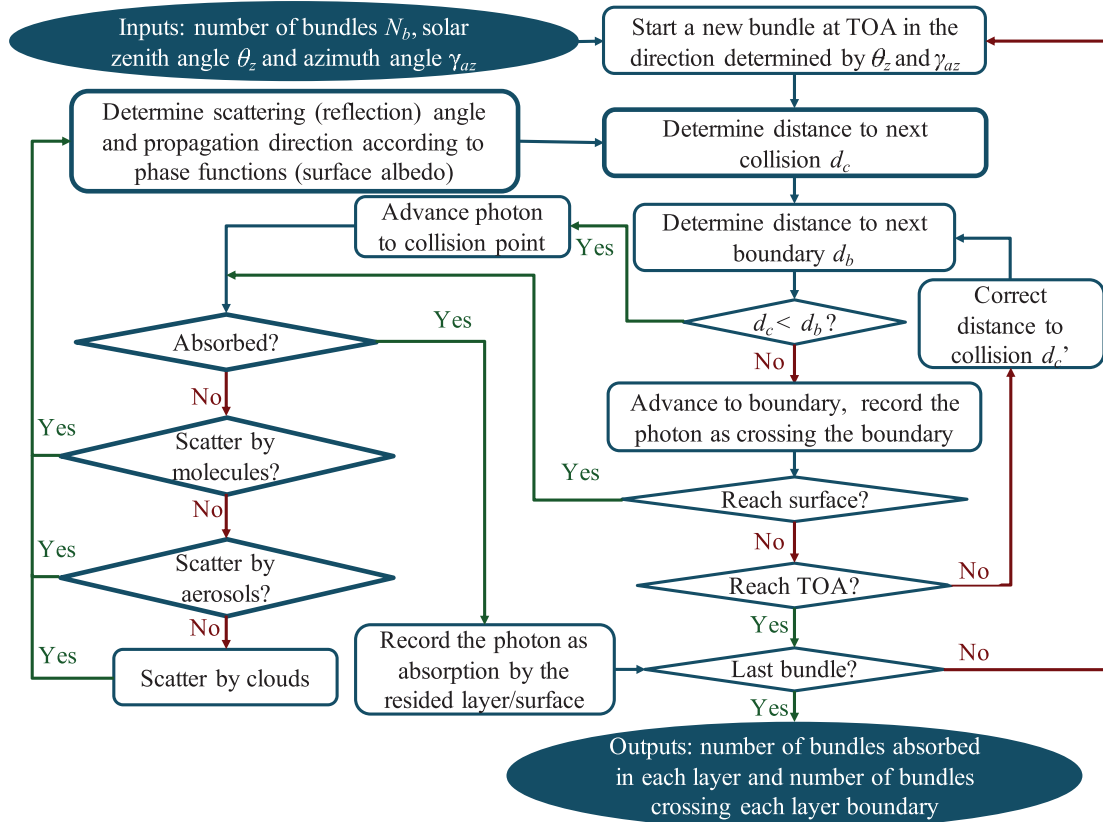


FIG. 2. Algorithm flow chart for the MC radiative transfer model used in this work. Processes in the rectangles with thick lines use random number generators.

0 to 1). The photon traveling distance to the next collision d_c (m) is then

$$d_c = \frac{\tau_0}{\kappa_e} = -\frac{\ln \xi_{\tau_0}}{\kappa_e}, \quad (9)$$

where κ_e (cm^{-1}) is the monochromatic extinction coefficient of the atmospheric layer within which the photon travels.

The distance to the nearest boundary d_b (m) in the direction of photon propagation is, then, calculated. For a plane-parallel geometry,

$$d_b = \left| \frac{z_b - z}{r_z} \right|, \quad (10)$$

where z_b (m) is the location of the nearest boundary in the photon traveling direction and z is the current location of the photon. If $d_c < d_b$, the collision happens in the current layer. Otherwise, the photon advances to the boundary with its coordinates updated as

$$x' = x + r_x d_b; \quad y' = y + r_y d_b; \quad z' = z + r_z d_b. \quad (11)$$

When a photon reaches a boundary, its energy is recorded as crossing the boundary, thus contributing to both the upwelling or downwelling fluxes. If the boundary is the ground surface, the photon interacts with the surface, being either absorbed or reflected back to the atmosphere. If the boundary is the top of the atmosphere (TOA),

the photon energy is recorded as outgoing energy. If the boundary is internal, the photon continues to propagate into the next layer. The distance to the next collision d'_c and to the next boundary d'_b is updated according to the optical properties of the new layer,

$$d'_c = \frac{\kappa_e}{\kappa'_e} (d_c - d_b), \quad d'_b = \left| \frac{z'_b - z_b}{r_z} \right|, \quad (12)$$

where κ'_e (cm^{-1}) is the extinction coefficient in the new (just-entered) layer. The updated distances d'_c and d'_b are, then, compared to determine whether the photon will interact within the layer or continue to travel to the next layer. This process continues until the photon collides with particles or exits the external boundaries.³⁶

2. Photon interactions with particles

When the photon collides with particles (gases or aerosols, including cloud droplets and ice crystals) in an atmosphere layer, the probabilities of being absorbed and scattered are

$$\begin{aligned} \text{Being scattered :} & \quad \xi_s \leq \sim \rho = \frac{\kappa_s}{\kappa_e}, \\ \text{Being absorbed :} & \quad \xi_s > \sim \rho, \end{aligned} \quad (13)$$

where κ_s (cm^{-1}) and κ_e (cm^{-1}) are scattering and extinction coefficients of that layer, respectively. If absorbed, the photon's lifetime

reaches the end, and its energy is converted to the thermal field of the layer. If scattered, the probability of being scattered by gas molecules, aerosols, and clouds is determined by

$$\begin{aligned} \text{Scattered by molecules: } & \zeta_h \leq \frac{\kappa_{s,\text{gas}}}{\kappa_s}, \\ \text{Scattered by aerosols: } & \frac{\kappa_{s,\text{gas}}}{\kappa_s} < \zeta_h \leq \frac{\kappa_{s,\text{gas}} + \kappa_{s,\text{aer}}}{\kappa_s}, \\ \text{Scattered by clouds: } & \zeta_h > \frac{\kappa_{s,\text{gas}} + \kappa_{s,\text{aer}}}{\kappa_s}, \end{aligned} \quad (14)$$

where $\kappa_{s,\text{gas}}$ (cm^{-1}) and $\kappa_{s,\text{aer}}$ (cm^{-1}) are the scattering coefficients of gases and aerosols, respectively.

After being scattered, the traveling direction of the photon is changed according to the scattering phase functions

$$\begin{aligned} \text{Rayleigh: } & P(\cos \Theta) = \frac{3}{4}(1 + \cos^2 \Theta), \\ \text{H-G: } & P(\cos \Theta) = \frac{1 - e_g^2}{2(1 + e_g^2 - 2e_g \cos \Theta)^{3/2}}, \end{aligned} \quad (15)$$

where Θ (rad) is the scattering angle and e_g is the scattering asymmetry parameter of the particles. For aerosols and clouds, the Henyey-Greenstein (H-G) scattering phase function is used to approximately model Mie scattering phenomena.³⁷ The scattering angle is sampled by inverting the cumulative phase function³⁷⁻³⁹

$$\begin{aligned} \zeta_\mu &= \int_{-1}^{\mu} P(\mu') d\mu', \\ \text{Rayleigh: } & \cos \Theta = \sqrt[3]{4\zeta_\mu - 2 + \sqrt{(4\zeta_\mu - 2)^2 + 1}} \\ & \quad + \sqrt[3]{4\zeta_\mu - 2 - \sqrt{(4\zeta_\mu - 2)^2 + 1}}, \\ \text{H-G: } & \cos \Theta = \frac{1}{2e_g} \left(1 + e_g^2 - \left(\frac{1 - e_g^2}{1 - e_g + 2e_g \zeta_\mu} \right)^2 \right), \end{aligned} \quad (16)$$

where $\mu = \cos \Theta$. With the sampled scattering zenith angle Θ and azimuth angle $\Phi = 2\pi\zeta_\Phi$, the photon traveling direction (r'_x , r'_y , r'_z) is updated to be⁴⁰

$$\begin{aligned} r'_x &= r_x \cos \Theta - \frac{\sin \Theta}{\sqrt{1 - r_z^2}} (r_x r_z \cos \Phi + r_y \sin \Phi), \\ r'_y &= r_y \cos \Theta - \frac{\sin \Theta}{\sqrt{1 - r_z^2}} (r_y r_z \cos \Phi - r_x \sin \Phi), \\ r'_z &= r_z \cos \Theta + \sqrt{1 - r_z^2} \sin \Theta \cos \Phi. \end{aligned} \quad (17)$$

The photon, then, travels in a new direction (r'_x , r'_y , r'_z) to the next collision location. The procedure repeats until the end of the photon's lifetime (when the photon is either absorbed or escapes to outer space).

3. Photon interactions with horizontal surfaces

When a photon reaches the horizontal ground, it will be either absorbed by the surface or reflected back to the atmosphere. For real surfaces (grass, snow, soil, etc.) and photovoltaic panels, the reflection

is modeled as diffuse reflection. For heliostats and other reflective surfaces in concentrated solar farms, specular reflections are assumed. The traveling direction of the photon after surface reflection is sampled as

$$\begin{aligned} \text{Diffuse reflection: } & r'_z = \sqrt{\zeta_z}, \\ \text{Specular reflection: } & r'_z = -r_z. \end{aligned} \quad (18)$$

Again, reflected photons continue to travel in the atmosphere until the end of its lifetime.

D. Fluxes on inclined surfaces

The solar irradiance on inclined surfaces is the summation of in-plane direct irradiance (G_i), in-plane diffuse irradiance (D_c), and irradiance due to ground reflection (D_g),¹

$$G_c = G_i + D_c + D_g. \quad (19)$$

G_i can be calculated directly by

$$G_i = G_d \cos \theta_i, \quad (20)$$

where G_d is the direct normal irradiance (DNI) and θ_i is the incidence angle,³

$$\cos \theta_i = \cos \theta_z \cos \beta + \sin \theta_z \sin \beta \cos (\gamma_{az} - \gamma_s). \quad (21)$$

In Eq. (21), θ_z is the solar beam zenith angle, β is the slope of the surface, γ_{az} is the solar beam azimuth angle, and γ_s is the surface azimuth angle. Figure 3 illustrates the different angles for an inclined surface.

While G_i is calculated deterministically from G_d , the values of D_c and D_g are either calculated from global horizontal irradiance (G_h) and diffuse horizontal irradiance (D_h) values by empirical transposition models (see the Appendix) or directly computed from Monte Carlo simulations.

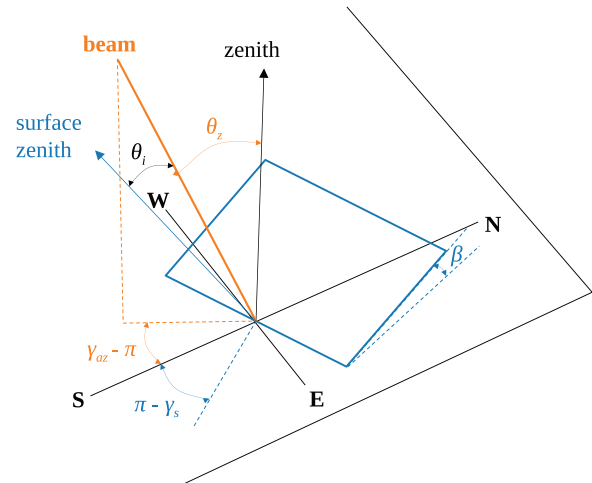


FIG. 3. Illustration of solar/beam zenith θ_z , azimuth γ_{az} , and incidence angles with surface tilt β and azimuth angle γ_s . This figure uses the same general notation as the standard reference.³

The Monte Carlo method calculates fluxes by tracing a certain amount of photons in bundles. Not only the number of photons crossing a boundary but also the crossing direction (r_x, r_y, r_z) of each photon needs to be computed. For downward traveling photons that reach the horizontal ground and for upward traveling photons reflected from the ground, the crossing zenith and azimuth angles are

$$\begin{aligned} \theta_p &= \cos^{-1} r_z, \quad \theta_p \in [0, \pi], \\ \gamma'_p &= \cos^{-1} \frac{r_x}{\sin \theta_p}, \quad \gamma'_p \in [0, \pi], \\ \gamma_p &= \begin{cases} \gamma'_p, & \text{if } r_y / \sin \theta_p > 0 \\ 2\pi - \gamma'_p, & \text{otherwise.} \end{cases} \end{aligned} \quad (22)$$

The incident angle of photons striking an inclined surface is calculated using Eq. (21) with θ_z and θ_{az} now replaced by θ_p and γ_p . The photon is counted as irradiance on the inclined surface if its incidence angle is smaller than 90° . The flux contribution from the photons that incident on the inclined surface is calculated as

$$e'_\nu = e_\nu \frac{\cos \theta_{i,p}}{\cos \theta_{i0,p}}, \quad (23)$$

where e_ν is the energy carried per photon as determined by Eq. (5), $\cos \theta_{i,p}$ is the cosine of the photon incidence angle on the inclined surface, and $\cos \theta_{i0,p}$ is the cosine of the photon incidence angle on the horizontal surface, which equals r_z .

E. Computational performance

Our Monte Carlo model was coded in Cython to achieve the readability provided by Python and the computational speed provided by C.⁴¹ For a cloudy 54-layer multiple scattering atmosphere with a spectral resolution of 3 cm^{-1} , tracking 1000 photons per wavenumber bandwidth (total of 10×10^6 photons) requires around 100 s of Intel Genuine CPU time with nine-core parallel computing enabled. This computation time allows the model to be used in real-time applications that require high accuracy and detailed knowledge about the spectral and directional radiative intensities.

III. VALIDATION OF THE RADIATIVE MODEL

A. Grid optimization

The accuracy of our Monte Carlo radiative transfer approach increases with the number of plane-parallel layers N_l , the number of spectral bandwidths (spectral grid) N_ν , and the number of photon bundles computed N_b . The computational cost increases linearly with N_ν and N_b and near linearly with N_l . In order to balance accuracy and computational costs, we performed a grid convergence study and found the minimum values of the product $N_l N_\nu N_b$, which result in errors within $\pm 1 \text{ W m}^{-2}$ for broadband surface global horizontal irradiance (GHI), surface direct normal irradiance (DNI), and both TOA and surface upwelling fluxes. Figure 4 presents the results for the grid convergence test using the AFGL midlatitude summer cloud-free atmosphere, a solar zenith angle of 30° , a surface relative humidity of 70%, and an aerosol optical depth at 497.5 nm (AOD) of 0.1. As shown in Fig. 4, a 54-layer atmosphere, with a spectral resolution of 3 cm^{-1} , and 1000 photons for each wavenumber can achieve the desired accuracy while preserving the minimum values of the product

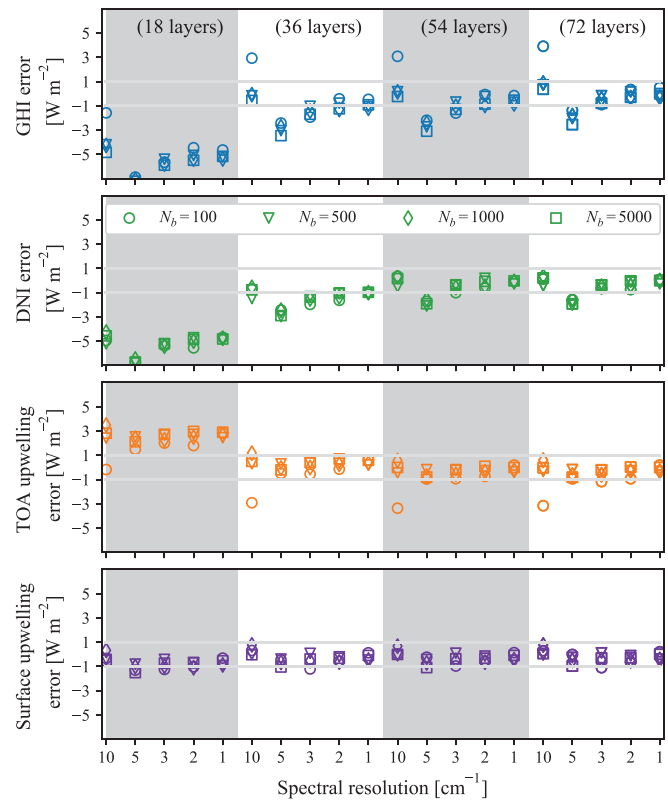


FIG. 4. Sample grid convergence test for Monte Carlo simulations. The target broadband tolerance is set to $\pm 1 \text{ W m}^{-2}$.

$N_l N_\nu N_b$. The troposphere (0–12 km of altitude) is represented by 39 layers.

B. Validation of irradiance on horizontal surfaces

The proposed MC radiative model is validated against shortwave modeling results from CHARTS radiative codes for six cases in the Continual Intercomparison of Radiation Codes (CIRC) program,⁴² using a spectral resolution of 3 cm^{-1} . Cases 1–4 are cloud-free, case 6 is cloudy with optically thick overcast liquid clouds, and case 7 is cloudy with moderately thin overcast liquid clouds. In our MC model, we adopt the inputs provided by the CIRC validation program: number of vertical layers, vertical pressure, temperature, and gas profiles, aerosol profiles, optical properties, cloud optical properties, solar zenith angle, spectral surface albedo, and extraterrestrial solar irradiance. The broadband flux comparisons are presented in Table I, showing that the results from the MC model are within 4% of downwelling flux and 9% of upwelling flux when compared with measurements and are of comparable accuracy of the CHARTS model. A spectral comparison between the MC model and CHARTS model is shown in Fig. 5. The spectral variation of the flux densities is comparable with the absolute difference lower than 20 mW cm m^{-2} for all wavenumbers, for downwelling and upwelling flux densities, and for clear and cloudy skies. Therefore, the MC model proposed here is suitable for simulating solar irradiance under various atmospheric conditions.

TABLE I. Comparison of results obtained by the proposed Monte Carlo model with measurements and the CHARTS model.

	Surface GHI (W m ⁻²)	Surface DNI (W m ⁻²)	TOA up (W m ⁻²)	Surface GHI error (%)	Surface DNI error (%)	TOA up error (%)
Case 1						
Measurements ⁴²	705.9	636.5	169.8			
CHARTS ⁴²	701.2	633.5	175.0	-0.67	-0.47	3.06
Monte Carlo model	703.7	636.5	175.4	-0.31	0.00	3.30
Case 2						
Measurements ⁴²	345.4	252.9	127.8			
CHARTS ⁴²	348.0	253.8	117.1	0.75	0.36	-8.37
Monte Carlo model	347.6	255.0	116.9	0.65	0.82	-8.52
Case 3						
Measurements ⁴²	772.5	674.5	159.6			
CHARTS ⁴²	773.1	675.1	173.6	0.08	0.09	8.77
Monte Carlo model	775.7	678.4	173.8	0.41	0.57	8.92
Case 4						
Measurements ⁴²	638.9	482.5	425.8			
CHARTS ⁴²	642.8	487.6	422.9	0.61	1.06	-0.68
Monte Carlo model	645.9	492.2	425.1	1.09	2.01	-0.16
Case 6						
Measurements ⁴²	97.6	0.8	623.2			
CHARTS ⁴²	92.1	0.0	628.8	-5.64	-100.00	0.90
Monte Carlo model	94.0	1.7	629.2	-3.67	110.52	0.96
Case 7						
Measurements ⁴²	479.8	8	356			
CHARTS ⁴²	473.7	0.1	356.4	-1.27	-98.75	0.11
Monte Carlo model	477.6	9.1	354.6	-0.46	13.17	-0.38

C. Validation of irradiance on inclined surfaces

Global horizontal (GHI) and plane of array (POA) irradiance values measured during clear sky periods at a utility-scale power plant in South-central California are used to validate the proposed Monte Carlo model in estimating solar irradiance values on inclined surfaces (i.e., the solar panels at the solar farm). The panels at this 250 MW plant are mounted on single axis trackers where the panel azimuth is due east in the morning and due west in the afternoon. The time varying tilt and azimuth angles of the panels are calculated using functions provided in the Python package pvlib.³³ The panel-to-ground ratio is 0.5 for this solar power plant. The clear sky Global Horizontal Irradiance (GHI_c), Direct Normal Irradiance (DNI_c), and Diffuse Horizontal Irradiance (DfHI_c) are computed using the Ineichen clear sky model.⁴³

In the Monte Carlo model, the AFGL midlatitude summer profile for the several atmospheric constituents is used with modifications to account for ambient air temperature and relative humidity.¹⁷ The AFGL midlatitude summer temperature profile is used with linear temperature adjustments in order to match the time varying temperatures at the surface.⁴⁴ Foreground albedo is set to be the same as CIRC case 2 for ground surfaces. Measurements of GHI under clear skies are used to infer the ambient aerosol optical depth (AOD) at 497.5 nm.

Figure 6 shows the comparison of measured and modeled GHI and POA for a representative clear day. Typical POA irradiance

deviations for any clear day out of the year using the Monte Carlo model are of the order of 5% when compared with measurements, and these discrepancies are mainly caused by the model atmosphere profiles, which is not always equal to the real local temperature and concentration profiles. For the comparison of POA irradiances computed by the Monte Carlo method and by the Perez4 transposition model, the Monte Carlo-generated GHI and DfHI irradiances are used as inputs to both models. This is done to allow for a direct comparison of the transposition component of the two models only. The proposed Monte Carlo model generally outperforms the Perez4 model in predicting clear sky POA irradiance fluxes. This strong performance of the MC method corroborates the methodology for flux calculation on inclined surfaces described in Sec. II D.

IV. RESULTS AND DISCUSSION

The model atmosphere used in this section has the following parameters: AFGL midlatitude summer temperature and constituent profiles with correction for surface constituent concentrations,¹⁷ an ambient relative humidity of 70%, an ambient AOD at 497.5 nm of 0.05, a solar zenith angle of $\theta_z = 30^\circ$, and an azimuth angle of $\gamma_{az} = 160^\circ$. For cloudy cases, model clouds are assumed to have a base height of 0.54 km, a thickness of 0.44 km, and a predefined optical depth (COD) at 497.5 nm.

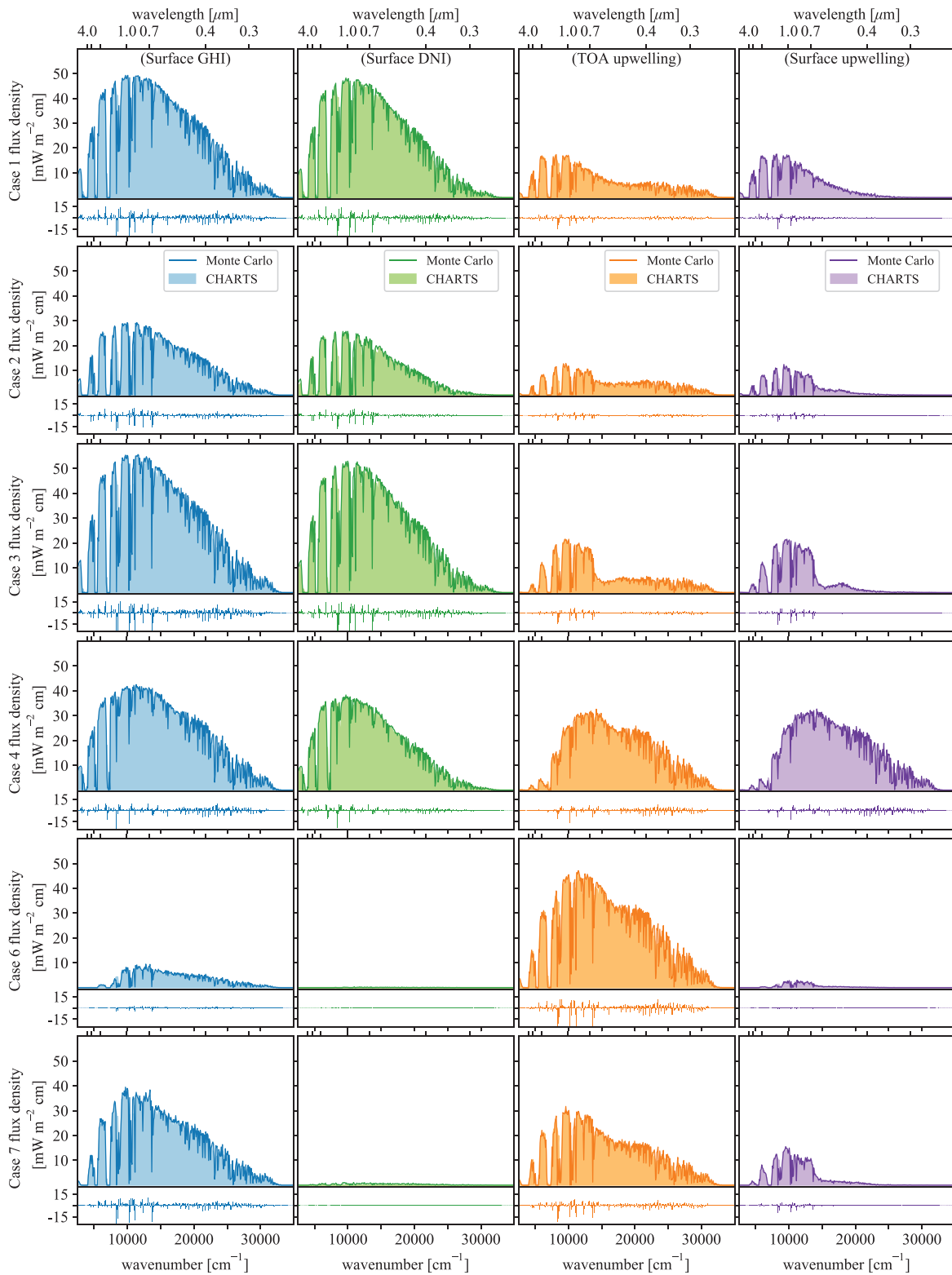


FIG. 5. Spectral comparison between the proposed MC model and the CHARTS model for six CIRC cases.

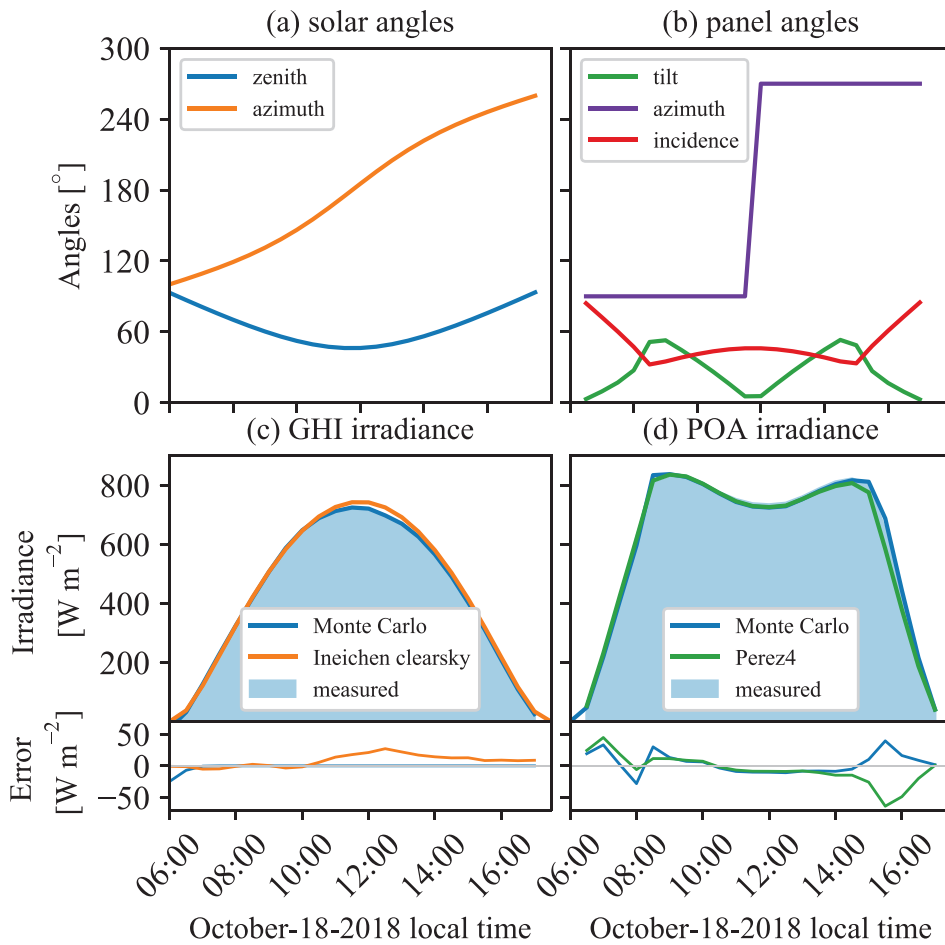


FIG. 6. Comparison of irradiance on inclined surfaces from the ground measurement and Monte Carlo (MC) simulations for a representative day (October 18, 2018). The POA irradiance results for the Perez4 model use MC-generated GHI and DNI as inputs. The main results shown in this figure are representative of many other clear days randomly selected throughout all for seasons for this particular location.

A. Angular distribution of broadband flux and intensity at horizontal surfaces

The broadband flux and intensity per angular bin ($\theta \pm d\theta/2, \gamma \pm d\gamma/2$) when measured at the horizontal surface are calculated as

$$F(\theta \pm d\theta/2, \gamma \pm d\gamma/2) = \int_{\nu_l}^{\nu_u} \frac{N_\nu(\theta \pm d\theta/2, \gamma \pm d\gamma/2) e_\nu}{d\theta d\gamma} d\nu, \quad (24)$$

$$I(\theta \pm d\theta/2, \gamma \pm d\gamma/2) = \int_{\nu_l}^{\nu_u} \frac{N_\nu(\theta \pm d\theta/2, \gamma \pm d\gamma/2) e_\nu}{\cos\theta d\omega} d\nu, \quad (25)$$

where ν_l and ν_u are the considered spectral limits, which are 2500 cm^{-1} and 35000 cm^{-1} , respectively. $N_\nu(\theta \pm d\theta/2, \gamma \pm d\gamma/2)$ is the number of photons reaching the ground in the direction of $(\theta \pm d\theta/2, \gamma \pm d\gamma/2)$ at wavenumber ν , e_ν is the energy per photon as defined in Eq. (5), and $d\omega$ is the unit solid angle, which is defined as $d\omega = \sin\theta d\theta d\gamma$.

The angular distribution of solar flux and intensity as measured on a horizontal surface are plotted in Figs. 7 and 8 for (a) clear sky, (b) overcast sky with COD = 1.0, and (c) overcast sky with COD = 10.0. The angular bin is shifted by γ_{az} for better illustration of azimuth symmetry.

In general, the angular flux is azimuth symmetric and decreases as angles deviate farther from solar angles. Under clear sky when the COD is zero, around 86.7% of the flux on the horizontal surface is direct, contributing to the bin of $(\theta_z \pm d\theta/2, \gamma_{az} \pm d\gamma/2)$. The remaining 13.3% flux is from photons that are scattered at least once by the cloudless atmosphere, so they reach the horizontal surface in a direction different from (θ_z, γ_{az}) . Due to the strong forward scattering nature of aerosols, the zenith spread of incident directions is confined within $\pm 30^\circ$, while the azimuth spread is within $\pm 45^\circ$. Under overcast skies with a (low) COD of 1.0, around 28.4% of the flux on the horizontal surface is in the direction of the solar beam. The remaining 71.6% of the flux is from photons that are scattered at least once. With the presence of clouds and especially at higher values of COD, multiple scattering events are more common, resulting in a larger spread of photon incident zenith and azimuth angles. Under overcast skies with a COD of 10.0, nearly all photons have been scattered at least once. Since the scattering azimuth angle is uniformly sampled from 0 to 2π , the azimuth incident angles of photons are symmetric, as shown in Fig. 7(c). Both clear sky and cloud aerosols produce strong forward scattering, so the photon zenith incident angles are concentrated around the solar zenith direction.

When plotting the angular distribution in terms of intensities (Fig. 8), horizon brightening ($\theta \rightarrow 90^\circ$) and circumsolar brightening

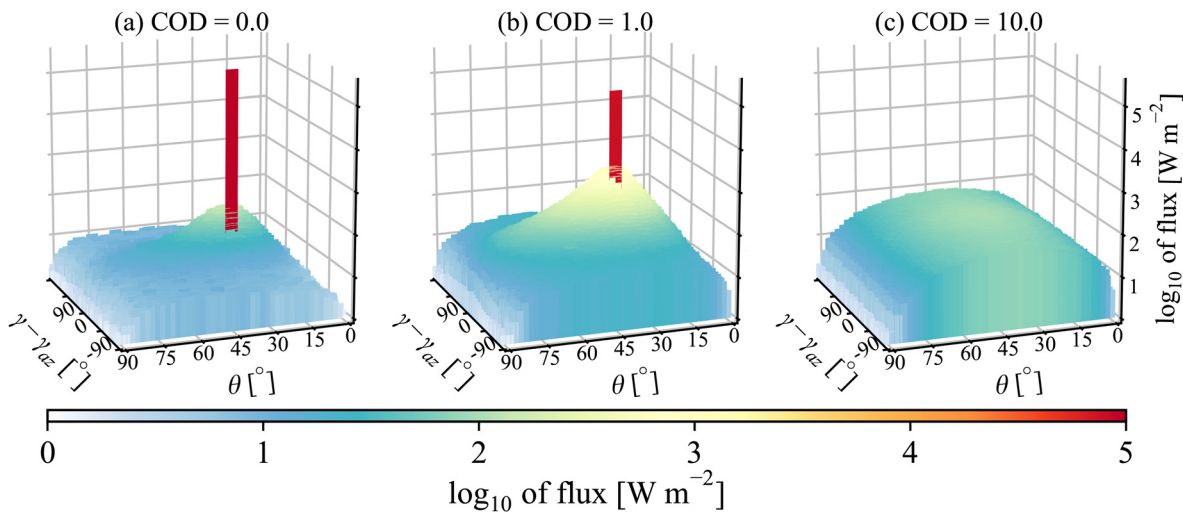


FIG. 7. Angular distribution of flux on horizontal surfaces for (a) clear skies, (b) overcast skies with a COD of 1.0, and (c) overcast skies with a COD of 10.0. The color scheme and the z-axis represent the flux per angular bin with $\delta\theta = 2^\circ$ and $\delta\gamma = 5^\circ$. For illustration, the \log_{10} of flux is plotted. When COD = 0.0 and 1.0, the flux is azimuth-symmetric and is the largest in the direction of the solar beam and decreases with increased $(\theta - \theta_z)$ and $(\gamma - \gamma_{az})$. When COD = 10.0, the flux is all diffuse, azimuth-independent, and zenith-symmetric.

effects ($\theta \rightarrow \theta_z$) are noticeable for clear sky and overcast sky with optically thin clouds. The horizon brightening is most profound under clear sky conditions, and even the presence of thin clouds diminishes substantially the brightening effect. For overcast skies with optically thick clouds, a mostly isotropic sky behavior is observed where the angular intensity is uniformly distributed, except for a slight difference in horizon darkening. The behavior of horizon brightening and darkening captured by the Monte Carlo model is in agreement with intensity measurements reported in the literature,⁵ which highlights the sensitivity of the proposed Monte Carlo model in discerning these secondary directional and spectral effects.

B. Comparisons with the Perez4 model

Empirical transposition models are developed to convert solar irradiance components on horizontal surfaces to irradiance on inclined surfaces. They typically take measured and/or modeled global horizontal irradiance (G_h) and diffuse horizontal irradiance (D_h) on the horizontal surface as inputs,

$$\begin{aligned} D_c &= D_h R_d, \\ D_g &= \rho_s G_h R_r, \end{aligned} \tag{26}$$

where R_d is the diffuse transposition factor, ρ_s is the foreground's albedo, and R_r is the transposition factors for the ground

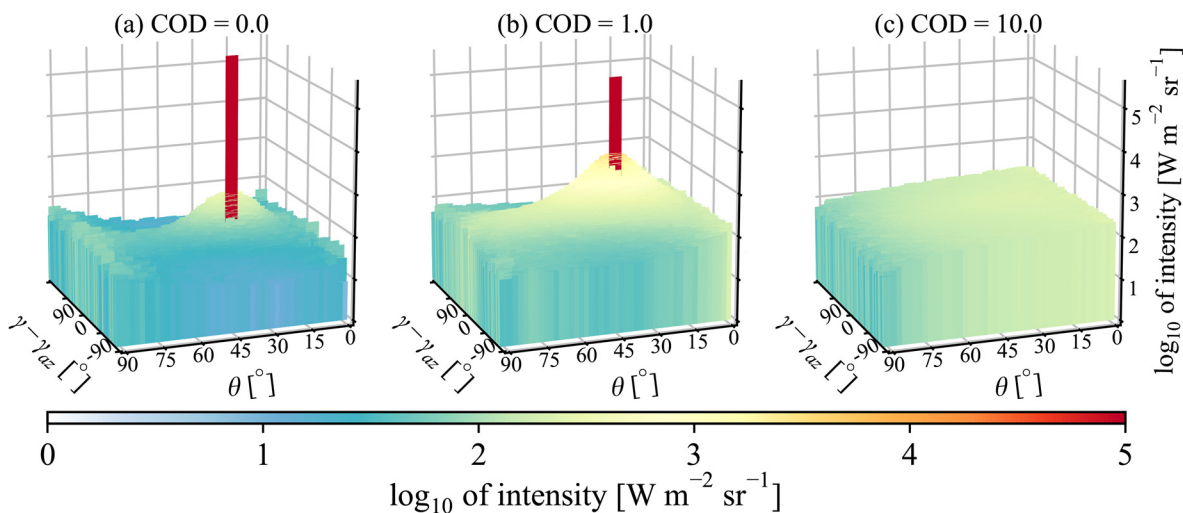


FIG. 8. Same as Fig. 7 but for the angular distribution of intensity. When COD = 0.0 and 1.0, the model successfully captures the horizon brightening, and the degree of brightening is weakened by the presence of clouds. When COD = 10.0, the irradiance is nearly isotropic with angular-independent intensity.

reflection, which is commonly modeled under the isotropic assumption,¹⁰

$$R_r = \frac{1 - \cos \beta}{2}. \quad (27)$$

The transposition factor R_d can be calculated using various transposition models [see Yang (2016)¹ for a comprehensive review]. The Perez4 model is found to perform better by Yang (2016)¹ and is, therefore, selected here for comparison with our Monte Carlo simulations. The formulation of the Perez4 model is reproduced in the Appendix for completeness.

1. Spectral comparisons

Figure 9 plots the spectral comparisons of plane of array irradiance (POA) between Monte Carlo simulations (Sec. IID) and the Perez4 transposition model (Appendix) for different surface inclinations β and azimuth angles γ_s . The inputs to the Perez4 models are Monte Carlo modeled GHI, DNI, and DfHI. Different rows represent different cloud optical depths, which quantifies how scattered the atmosphere is. The absolute error (AE) and relative error (RE) are defined as

$$\begin{aligned} AE &= POA_{\text{Perez4}} - POA_{\text{MC}}, \\ RE &= \frac{AE}{POA_{\text{MC}}}. \end{aligned} \quad (28)$$

The in-plane direct irradiance G_i and ground reflection D_g are the same for Monte Carlo and Perez4 models because G_i is deterministic and D_g is based on the same “isotropic reflection ground” assumption. The difference between the Monte Carlo and Perez4 models in estimating POA is caused by the sky diffuse component D_c .

The Perez4 empirical transposition model made general assumptions about the angular distribution of sky diffuse irradiance, which causes small POA error under clear skies because of the smaller values for the sky diffuse component. The Perez4 results deviate from MC simulations under cloudy skies for high surface inclination angles. The spectral differences reside mostly in the range between 5000 and 25000 cm^{-1} , the portion of the spectrum where scattering plays an important role. In this range, the angular distribution of diffuse irradiance is strongly dependent on local atmospheric conditions. When $\text{COD} = 1.0$, the clouds are optically thin so that multiple scattering is not common. Due to the forward scattering nature of clouds, most photons travel in the direction close to the direction of the solar beam (see also Fig. 8), making the diffuse irradiance field anisotropic and

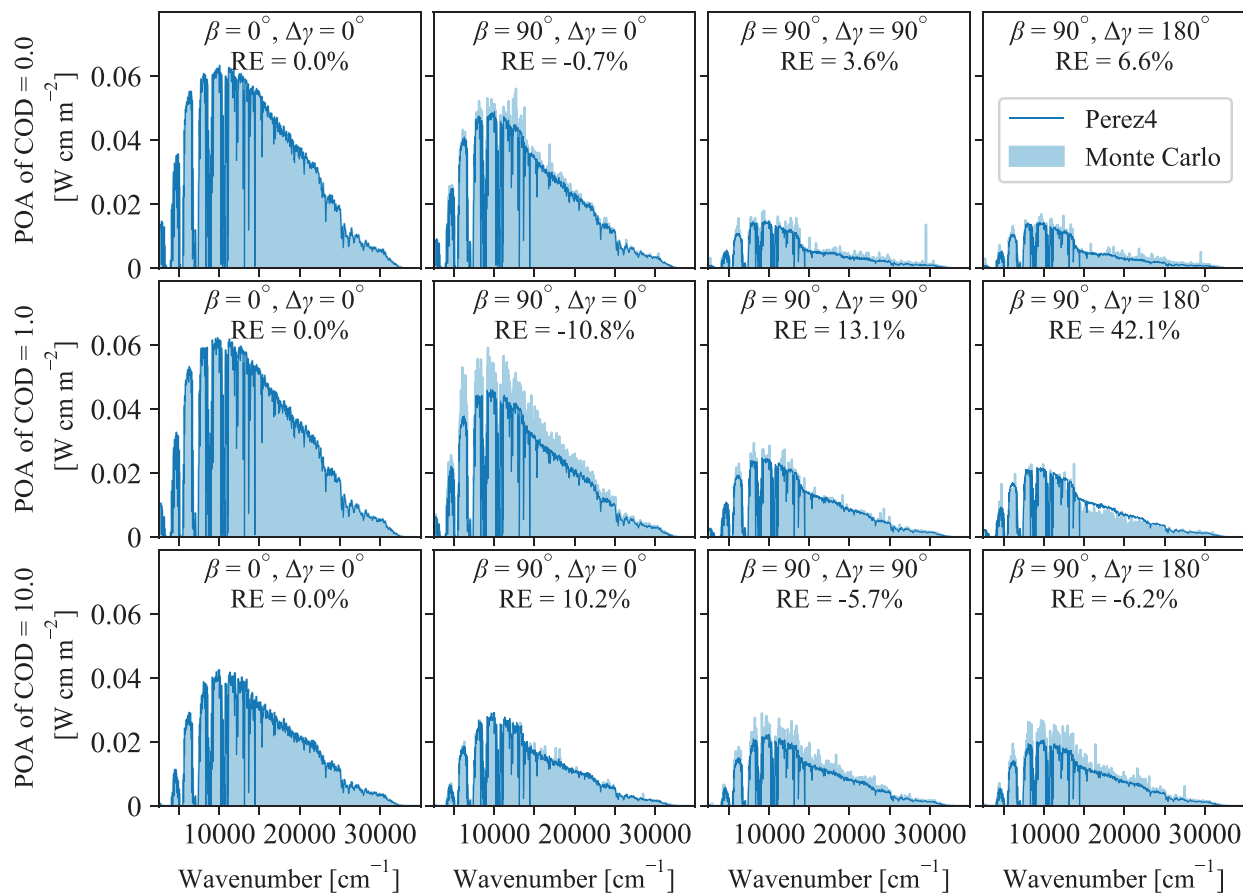


FIG. 9. Spectral comparisons of POA flux density between the Monte Carlo simulations and the Perez4 transposition model for different surface tilt angles β , the surface and solar azimuth angle difference $\Delta\gamma$, and the cloud optical depth (COD).

favoring the directions around the beam. The Perez4 model underestimates the anisotropy and thus underestimates the POA on inclined surfaces when β is large and $\Delta\gamma < 90^\circ$. While for large β and $\gamma > 90^\circ$, the Perez4 model overestimates the POA. When $COD = 10.0$, the clouds are optically thick, which induces frequent multi-scattering. So, the anisotropy of diffuse irradiance becomes smaller as does the deviation of the Perez4 model. Note that when $COD = 10.0$ and $\beta = 90^\circ$, the POA is nearly azimuth-independent as captured by the Monte Carlo model, but Perez4 introduces “artificial” anisotropy.

The Monte Carlo model is also able to capture different spectral variations of POA when compared with GHI. For example, when $\beta = 90^\circ$, $\Delta\gamma = 0^\circ$, and $COD = 0$, the POA between $10\,000$ and $13\,000\text{ cm}^{-1}$ is larger than that between $7\,000$ and $10\,000\text{ cm}^{-1}$, indicating that the scattering in the atmosphere within the spectral range $10\,000\text{--}13\,000\text{ cm}^{-1}$ is more favored in the directions close to the horizon with large $\cos\theta_p$. Other spikes in the Monte Carlo results are caused by more photons traveling in the directions near the horizon where they have a large $\cos\theta_p$ component.

2. Broadband comparisons

Figure 10 shows broadband comparisons of POA between the Monte Carlo simulations and the Perez4 transposition model. Different subplots refer to different cloud optical depths. In the top row, the POA values for both approaches are plotted. In the middle row, the absolute deviations (labeled AE) between the MC simulations and Perez4 model are plotted, and in the bottom row, the relative deviations (labeled RE) between the two models are plotted. In general, the match between the two models is very good, but the Perez4 model deviates more strongly with increasing surface β and $\Delta\gamma$. These deviations are consistent with the comparisons made with experimental data (Fig. 6). In general, the relative disagreement between the two models is smaller than 10% under clear sky conditions.

For optically thin clouds ($COD = 0.5$ and $COD = 1.0$), Perez4 underestimates the zenith-anisotropy of sky diffuse irradiance caused by forward scattering of clouds in comparison with the MC simulations. The models disagree (negative deviations) for $s\Delta\gamma < 90^\circ$ and also for $\Delta\gamma > 90^\circ$ (positive deviations). For optically thick clouds ($COD = 5.0$ and $COD = 10.0$), the deviations are smaller, especially

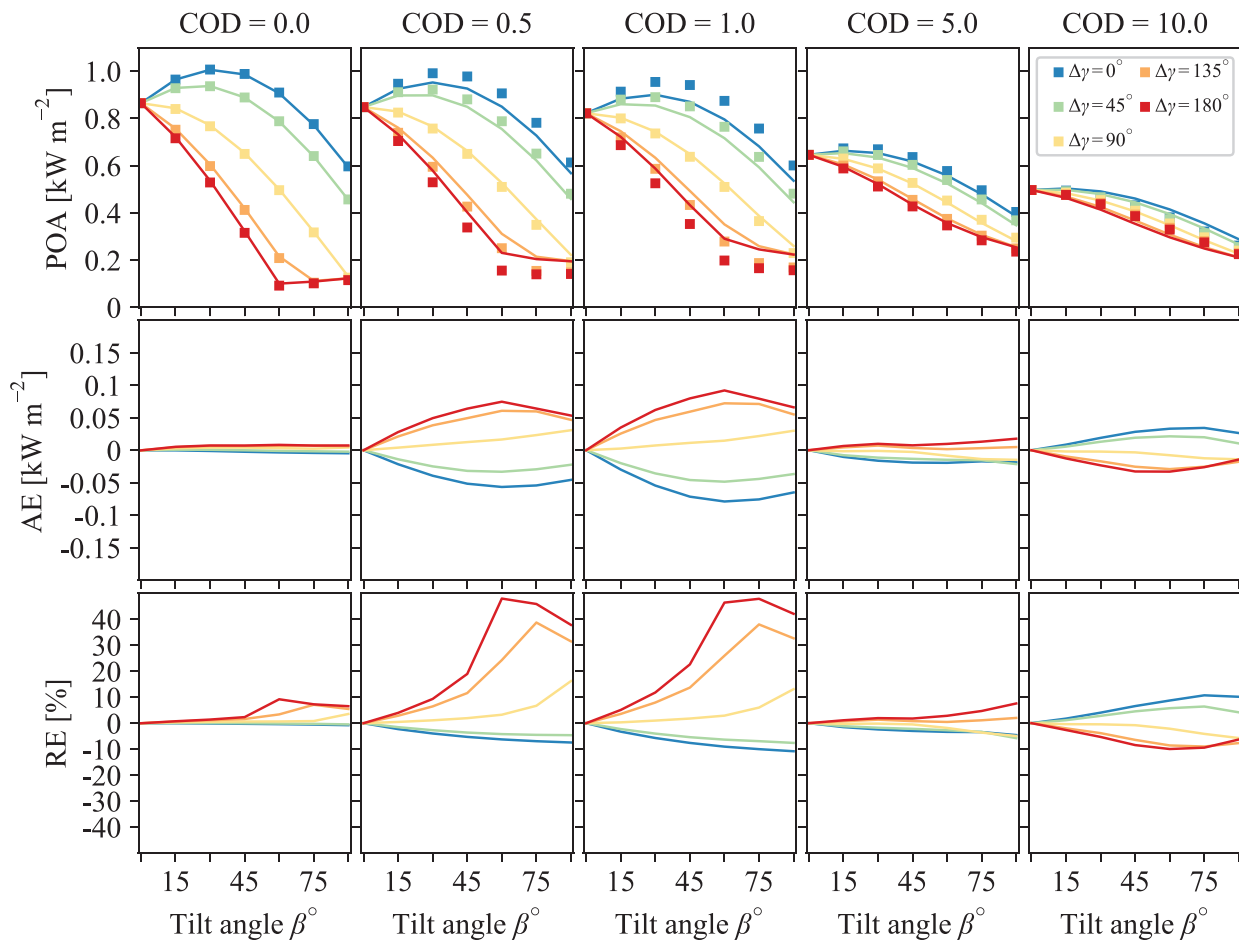


FIG. 10. Broadband comparisons between Monte Carlo simulations (symbols) and the Perez4 transposition model (solid lines), for different surface tilt angles β , the surface and solar azimuth angle difference $\Delta\gamma$, and the cloud optical depth (COD).

when compared to optically thin clouds, because the presence of multiple scattering of clouds reduces the azimuth-anisotropy and zenith-anisotropy of the sky diffuse irradiance. In sum, the general agreement between the two approaches is very high under clear skies and optically thick clouds, while larger deviations appear under optically thin clouds. The mean relative error between the two models is 6.02% (average of the absolute values of relative errors over all β , $\Delta\gamma$, and COD), which is consistent with other studies in the literature^{1,45} where the accuracy of the Perez4 model is estimated around 9% when compared against measurements.

V. CONCLUSIONS

Accurate estimation of spectral solar irradiance on inclined surfaces is important for the design and evaluation of concentrated solar and photovoltaic installations. Due to a lack of extensive measurements and detailed models for POA irradiance, various empirical transposition models have been proposed in the literature to simulate POA irradiance values from global horizontal irradiance (GHI) and diffuse horizontal irradiance (DfHI). However, POA depends on the anisotropic distribution of solar irradiance in the atmosphere, which, in turn, depends on local atmospheric conditions. Because of that, simple empirical transposition models with regressed coefficients are unable to accurately estimate the angular distribution of solar irradiance (and thus POA irradiance) under all sky conditions.

This work presents a comprehensive line-by-line Monte Carlo radiative transfer model to simulate solar irradiance through the atmosphere by statistically tracking photons. When a large number of photons are traced, the Monte Carlo model is able to reproduce the angular distribution of solar irradiance without any angular discretization, thus computing high fidelity POA irradiance values for surfaces with different orientations and optical properties. The model very closely resembles the physics involved and thus offers a way to study the effectiveness of other approaches. A 54-layer atmosphere, with a spectral resolution of 3 cm^{-1} and 1000 photons per wavenumber bandwidth, is found to achieve grid convergence while requiring minimum computational efforts. The proposed Monte Carlo model is validated against measurements and modeling results from the Continual Intercomparison of Radiation Codes program (CIRC), as well as POA irradiance measurements made at an operational, utility-scale, single-axis tracking solar farm in South-Central California.

When comparing the Monte Carlo model with the most widely accepted empirical transposition model (Perez4), we find both models in good agreement for small surface tilt angles β . Larger deviations are found as surface tilt angles increase. The deviation is also augmented when the difference between the solar and the surface azimuth angles $\Delta\gamma$ increases. Under clear skies, the deviation between the Perez4 model and the MC simulations is smaller than 10% for all possible surface tilt and azimuth angles. Under optically thin cloud conditions ($\text{COD} \leq 1.0$), the Perez4 model underestimates POA by 0%–10% when $\Delta\gamma < 90^\circ$ and overestimates POA by 0%–50% when $\Delta\gamma > 90^\circ$ when compared to the MC simulations. The error is more evident when $\beta > 45^\circ$. Under optically thick clouds ($\text{COD} \geq 5.0$), the agreement between the two approaches is smaller than 15% for most combinations of β and $\Delta\gamma$. Since the presence of optically thick clouds reduces the anisotropy of diffuse solar irradiance, the deviations between the two models are found to be smaller when compared with optically thin cloud cases. Deviations between the two models average

$\approx 6\%$ for all surface orientations and cloud optical depths considered, which strongly validates the use of the Perez4 model for financial and engineering performance analyses, especially at midrange latitudes and moderate tilt angles. Thus, the results presented in this study not only add strong support for the Perez4 model in solar applications but also highlight some of the limitations of empirical models for both high latitude installations and under certain cloud cover conditions that must be further examined.

When detailed atmospheric temperature and concentration profiles (including cloud optical properties) are available (e.g., derived from satellite imagery⁴⁴), the shortwave radiative model proposed here can be used to produce accurate POA irradiance values for various atmospheric conditions, different surface orientations, and ground and surface optical properties. Other more complex physical processes such as light polarization and soiling effects, as well as anisotropic surface and ground properties, can also be easily incorporated into the fast Monte Carlo method proposed in this study.

ACKNOWLEDGMENTS

The authors gratefully acknowledge partial support from the U.S. Department of Energy's Office of Energy Efficiency and Renewable Energy (EERE) under Solar Energy Technologies Office (SETO) Agreement No. EE0008216.

APPENDIX: THE PEREZ4 TRANSPOSITION MODEL

The empirical transposition factor R_d in the Perez4 model is expressed as⁷

$$R_d = (1 - F_1) \frac{1 + \cos \beta}{2} + F_1 \frac{a'}{c'} + F_2 \sin \beta, \quad (\text{A1})$$

where

$$\begin{aligned} a' &= 2(1 - \cos \alpha) \chi_c, \\ c' &= 2(1 - \cos \alpha) \chi_h, \end{aligned} \quad (\text{A2})$$

$$\chi_c = \begin{cases} \psi_h \cos \theta_i, & \text{if } \theta_i < \pi/2 - \alpha \\ \psi_h \psi_c \sin(\psi_c \alpha), & \text{if } \theta_i \in [\pi/2 \pm \alpha] \\ 0, & \text{otherwise,} \end{cases}$$

$$\chi_h = \begin{cases} \cos \theta_z, & \text{if } \theta_z < \pi/2 - \alpha \\ \psi_h \sin(\psi_h \alpha), & \text{otherwise,} \end{cases} \quad (\text{A3})$$

$$\psi_c = \frac{\pi/2 - \theta_i + \alpha}{2\alpha},$$

$$\psi_h = \begin{cases} (\pi/2 - \theta_z + \alpha)/2\alpha, & \text{if } \theta_z > \pi/2 - \alpha \\ 1, & \text{otherwise,} \end{cases} \quad (\text{A4})$$

$$\begin{aligned} F_1 &= \max(0, F_{11}(\epsilon') + \Delta F_{12}(\epsilon') + \theta_z F_{13}(\epsilon')), \\ F_2 &= F_{21}(\epsilon') + F_{22}(\epsilon') \Delta + F_{23}(\epsilon') \theta_z, \\ \epsilon' &= (D_h + I)/D_h, \\ \Delta &= D_h/(G_0 \cos \theta_z), \end{aligned} \quad (\text{A5})$$

and α is the circumsolar half angle, which is assumed to be 25° .⁷ G_0 is the extraterrestrial irradiance, and the values of coefficients F_{ij} are given in Table II.

TABLE II. Perez4 model coefficients for irradiance as a function of the sky's clearness ε .

ε'	F_{11}	F_{12}	F_{13}	F_{21}	F_{22}	F_{23}
[1, 1.065)	-0.008	0.588	-0.062	-0.060	0.072	-0.022
[1.065, 1.23)	0.130	0.683	-0.151	-0.019	0.066	-0.029
[1.23, 1.5)	0.330	0.487	-0.221	0.055	-0.064	-0.026
[1.5, 1.95)	0.568	0.187	-0.295	0.109	-0.152	-0.014
[1.95, 2.8)	0.873	-0.392	-0.362	0.226	-0.462	0.001
[2.8, 4.5)	1.133	-1.237	-0.412	0.288	-0.823	0.056
[4.5, 6.2)	1.060	-1.600	-0.359	0.264	-1.127	0.131
[6.2, $+\infty$)	0.678	0.327	0.250	0.156	1.377	0.251

DATA AVAILABILITY

The data that support the findings of this study are available from the corresponding author upon reasonable request.

REFERENCES

- D. Yang, "Solar radiation on inclined surfaces: Corrections and benchmarks," *Sol. Energy* **136**, 288–302 (2016).
- M. Lave and J. Kleissl, "Optimum fixed orientations and benefits of tracking for capturing solar radiation in the continental United States," *Renewable Energy* **36**, 1145–1152 (2011).
- J. A. Duffie and W. A. Beckman, *Solar Engineering of Thermal Processes*, 4th ed. (John Wiley & Sons Inc, Hoboken, New Jersey, 2013).
- K. J. Kondratyev and M. Manolova, "The radiation balance of slopes," *Sol. Energy* **4**, 14–19 (1960).
- J. Bugler, "The determination of hourly insolation on an inclined plane using a diffuse irradiance model based on hourly measured global horizontal insolation," *Sol. Energy* **19**, 477–491 (1977).
- J. E. Hay and D. C. McKay, "Estimating solar irradiance on inclined surfaces: A review and assessment of methodologies," *Int. J. Sol. Energy* **3**, 203–240 (1985).
- R. Perez, R. Seals, P. Ineichen, R. Stewart, and D. Menicucci, "A new simplified version of the Perez diffuse irradiance model for tilted surfaces," *Sol. Energy* **39**, 221–231 (1987).
- C. A. Gueymard, "An anisotropic solar irradiance model for tilted surfaces and its comparison with selected engineering algorithms," *Sol. Energy* **38**, 367–386 (1987).
- K. N. Liou, *An Introduction to Atmospheric Radiation* (Academic Press, Cambridge, MA, USA, 2002), Vol. 84.
- C. A. Gueymard, "Direct and indirect uncertainties in the prediction of tilted irradiance for solar engineering applications," *Sol. Energy* **83**, 432–444 (2009).
- A. Souza and J. F. Escobedo, "Estimates of hourly diffuse radiation on tilted surfaces in Southeast of Brazil," *Int. J. Renewable Energy Res.* **3**, 207–221 (2013).
- R. Wattan and S. Janjai, "An investigation of the performance of 14 models for estimating hourly diffuse irradiation on inclined surfaces at tropical sites," *Renewable Energy* **93**, 667–674 (2016).
- E. J. Mlawer, S. J. Taubman, P. D. Brown, M. J. Iacono, and S. A. Clough, "Radiative transfer for inhomogeneous atmospheres: RRTM, a validated correlated-k model for the longwave," *J. Geophys. Res.* **102**, 16663–16682, <https://doi.org/10.1029/97JD00237> (1997).
- S. Kato, T. P. Ackerman, J. H. Mather, and E. E. Clothiaux, "The k-distribution method and correlated-k approximation for a shortwave radiative transfer model," *J. Quant. Spectrosc. Radiat. Transfer* **62**, 109–121 (1999).
- K. Stamnes, S.-C. Tsay, W. Wiscombe, and I. Laszlo, "DISORT, a general-purpose Fortran program for discrete-ordinate-method radiative transfer in scattering and emitting layered media: Documentation of methodology" (Department of Physics and Engineering Physics, Stevens Institute of Technology, 2000).
- S. Clough, M. Shephard, E. Mlawer, J. Delamere, M. Iacono, K. Cady-Pereira, S. Boukabara, and P. Brown, "Atmospheric radiative transfer modeling: A summary of the AER codes," *J. Quant. Spectrosc. Radiat. Transfer* **91**, 233–244 (2005).
- M. Li, Z. Liao, and C. F. M. Coimbra, "Spectral model for clear sky atmospheric longwave radiation," *J. Quant. Spectrosc. Radiat. Transfer* **209**, 196–211 (2018).
- K. Stamnes, S. Tsai, W. Wiscombe, and K. Jayaweera, "Numerically stable algorithm for discrete-ordinate-method radiative transfer in multiple scattering and emitting layered media," *Appl. Opt.* **27**, 2502–2509 (1988).
- Z. Lin, S. Stamnes, J. Lin, I. Laszlo, S. C. Tsai, W. Wiscombe, and K. Stamnes, "Improved discrete ordinate solutions in the presence of an anisotropically reflecting lower boundary: Upgrades of the DISORT computational tool," *J. Quant. Spectrosc. Radiat. Transfer* **157**, 119–134 (2015).
- D. Cohen, S. Stamnes, T. Tanikawa, E. Sommersten, J. Stamnes, J. Lotsberg, and K. Stamnes, "Comparison of discrete ordinate and Monte Carlo simulations of polarized radiative transfer in two coupled slabs with different refractive indices," *Opt. Express* **21**, 9592–9614 (2013).
- C. A. Gueymard, "Prediction and validation of cloudless shortwave solar spectra incident on horizontal, tilted, or tracking surfaces," *Sol. Energy* **82**, 260–271 (2008).
- Y. Xie and S. Mengupta, "A fast all-sky radiation model for solar applications with narrowband irradiances on tilted surfaces (FARMS-NIT): Part I. The clear-sky model," *Sol. Energy* **174**, 691–702 (2018).
- Y. Xie and S. Mengupta, "A fast all-sky radiation model for solar applications with narrowband irradiances on tilted surfaces (FARMS-NIT): Part II. The cloudy-sky model," *Sol. Energy* **188**, 799–812 (2019).
- Z. Liao, M. Li, and C. F. M. Coimbra, "Anisotropic corrections for the downwelling radiative heat transfer flux from various types of aerosols," *Int. J. Heat Mass Transfer* **136**, 1006–1016 (2019).
- G. P. Anderson, S. A. Clough, F. X. Kneizys, J. H. Chetwynd, and E. P. Shettle, "AFGL atmospheric constituent profiles (0.120 km)," Technical Report No. 954 AFGL-TR-86-0110 (DTIC Document, 1986).
- I. B. Pollack, T. B. Ryerson, M. Trainer, J. Neuman, J. M. Roberts, and D. D. Parrish, "Trends in ozone, its precursors, and related secondary oxidation products in Los Angeles, California: A synthesis of measurements from 1960 to 2010," *J. Geophys. Res.* **118**, 5893–5911, <https://doi.org/10.1002/jgrd.50472> (2013).
- M. Li and C. F. M. Coimbra, "On the effective spectral emissivity of clear skies and the radiative cooling potential of selectively designed materials," *Int. J. Heat Mass Transfer* **135**, 1053–1062 (2019).
- R. V. Kochanov, I. E. Gordon, L. S. Rothman, P. Wcislo, C. Hill, and J. S. Wilzewski, "HITRAN application programming interface (HAPI): A comprehensive approach to working with spectroscopic data," *J. Quant. Spectrosc. Radiat. Transfer* **177**, 15–30 (2016).
- E. J. Mlawer, V. H. Payne, J.-L. Moncet, J. S. Delamere, M. J. Alvarado, and D. C. Tobin, "Development and recent evaluation of the MT_CKD model of continuum absorption," *Philos. Trans. R. Soc., London A* **370**, 2520–2556 (2012).
- M. Li, H. B. Peterson, and C. F. M. Coimbra, "Radiative cooling resource maps for the contiguous United States," *J. Renewable Sustainable Energy* **11**, 036501 (2019).
- A. Bucholtz, "Rayleigh-scattering calculations for the terrestrial atmosphere," *Appl. Opt.* **34**, 2765–2773 (1995).
- E. R. Peck and K. Reeder, "Dispersion of air," *JOSA* **62**, 958–962 (1972).
- W. F. Holmgren, C. W. Hansen, and M. A. Mikofski, "pvlib python: A python package for modeling solar energy systems," *J. Open Source Software* **3**, 884 (2018).
- F. Kastan and A. T. Young, "Revised optical air mass tables and approximation formula," *Appl. Opt.* **28**, 4735–4738 (1989).
- See <https://www.nrel.gov/grid/solar-resource/spectra-astm-e490.html> for "National Renewable Energy Laboratory, 2000 ASTM Standard Extraterrestrial Spectrum Reference E-490-00."
- L. House and L. Avery, "The Monte Carlo technique applied to radiative transfer," *J. Quant. Spectrosc. Radiat. Transfer* **9**, 1579–1591 (1969).
- D. Toublanc, "Henyey-Greenstein and Mie phase functions in Monte Carlo radiative transfer computations," *Appl. Opt.* **35**, 3270–3274 (1996).
- J. R. Frisvad, "Importance sampling the Rayleigh phase function," *J. Opt. Soc. Am. A* **28**, 2436–2441 (2011).

- ³⁹K. I. Gjerstad, J. J. Stamnes, B. Hamre, J. K. Lotsberg, B. Yan, and K. Stamnes, "Monte Carlo and discrete-ordinate simulations of irradiances in the coupled atmosphere-ocean system," *Appl. Opt.* **42**, 2609–2622 (2003).
- ⁴⁰O. N. Vassiliev, "Monte Carlo methods for radiation transport," *Fundamentals and Advanced Topics* (Springer, Cham, 2017).
- ⁴¹S. Behnel, R. Bradshaw, C. Citro, L. Dalcin, D. S. Seljebotn, and K. Smith, "Cython: The best of both worlds," *Comput. Sci. Eng.* **13**, 31 (2011).
- ⁴²See <https://circ.gsfc.nasa.gov/> for "National Oceanic and Atmospheric Administration, CIRC: Continual Intercomparison of Radiation Codes."
- ⁴³P. Ineichen and R. Perez, "A new airmass independent formulation for the Linke turbidity coefficient," *Sol. Energy* **73**, 151–157 (2002).
- ⁴⁴D. P. Larson, M. Li, and C. F. M. Coimbra, "SCOPE: Spectral cloud optical property estimation using real-time GOES-R longwave imagery," *J. Renewable Sustainable Energy* **12**, 026501 (2020).
- ⁴⁵P. Loutzenhiser, H. Manz, C. Felsmann, P. Strachan, T. Frank, and G. Maxwell, "Empirical validation of models to compute solar irradiance on inclined surfaces for building energy simulation," *Sol. Energy* **81**, 254–267 (2007).